Annual Progress Report,

covering the period

1 September 1974 to 31 August 1975

for

GRANT NGR 05017027

entitled

STUDIES IN MATTER ANTIMATTER SEPARATION AND IN THE ORIGIN OF LUNAR MAGNETISM

conducted by

William A. Barker, Principal Investigator

Ronald Greeley, Curtis Parkin, Hans Aggarwal, and Peter Schultz
Coinvestigators

University of Santa Clara
California 95053

The NASA Technical Officer for this grant is
Dr. W. Quaide, Space Sciences Division,
Ames Research Center, NASA, Moffett Field, CA. 94035

32 Pages Total

I. Introduction

This is a six-month progress report covering lunar and planetary research conducted by five investigators. The specific objectives, approaches, and statements of work are presented in the bodies of the proposals submitted in August 1974 and March 1975.

II. Summaries of Progress

In the following sections, the progress completed by each investigator is summarized. In addition, abstracts of papers published, in press, manuscripts, or formal oral presentations are included following each investigator's synopsis of the research completed.

A. DR. WILLIAM A. BARKER: Studies of Lunar Magnetism.

During this report period, progress was made in better defining a model of the lunar ionosphere. The results of this work will be presented at the Fall Meeting of the American Geophysical Union and are summarized in the following abstract.

Publication:

1. W. D. Daily, W. A. Barker, P. Dyal, and C. W. Parkin, "A Model Lunar Ionosphere for the Moon in the Geomagnetic Tail."

A MODEL LUNAR IONOSPHERE FOR THE MOON IN THE GEOMAGNETIC TAIL

W.D. Daily (Dept. of Physics and Astronomy, Brigham Young Univ., Provo, Utah 84602)
W.A. Barker (Dept. of Physics, U. of Santa Clara, Santa Clara, California 95053)
P. Dyal (Space Science Div., NASA-Ames Research Center, Moffett Field, California 94035)
C.W. Parkin (Dept. of Physics, U. of Santa Clara, Santa Clara, California 95053)

Previous models of the lunar ionosphere have been confined to times when the moon is in the solar wind. In this paper we describe a model lunar ionosphere for conditions when the moon is shielded from the solar wind by the geomagnetosphere. In the solar wind the lighter elements of He, H_2 and H are significant components of the lunar atmosphere. In addition, this atmosphere is ionized principally by charge exchange, and the motional electric field of the solar wind is responsible for the loss rate of the ionosphere from the moon. On the other hand, during the four days of each lunation when the moon is in the geomagnetic field, the He, H_2 and H thermally escape and do not contribute significantly to the atmosphere. Ne and Ar become the main atmospheric components. This atmosphere is photoionized, resulting in ions which are essentially in thermal equilibrium with the lunar surface (300°K); and electrons are calculated to have energies of approximately 20eV. These high energy electrons would escape very rapidly except that charge neutrality requires that they be restrained by the low energy ions. Theoretical results will be presented for scale height of the lunar ionosphere as a function of electron temperature and ion mass. An estimate is obtained for the mean lifetime of ions and electrons, and the ion density near the surface is calculated to be ~ 0.2 cm^{-3}. The ionosphere is a diamagnetic plasma and near 100 km altitude it is characterized by a magnetic permeability of ~ 0.8.

B. DR. RONALD GREELEY: Studies in Lunar and Planetary Geology.

The following tasks were completed during the grant period:

1) Low Pressure Wind Tunnel for Simulations of the Martian Aeolian Environment. During the grant period the basic wind tunnel shell has been constructed and installed in the low pressure chamber. After an initial problem of design for the ejector drive system, a suitable array of nozzles for the ejector system has been devised and was installed in September, 1975. Basic instrumentation for the measurement of wind velocity within the tunnel has been completed and is currently undergoing a systems checkout. Close-circuit, high resolution television monitoring system for detecting threshold of particle movement within the tunnel is half completed and the system is currently awaiting delivery of the television monitor. It is anticipated that initial threshold experiments will begin in November or December of this year.

2) Application of Wind Tunnel Simulations to Martian Aeolian Problems. Using the data obtained from earlier atmospheric wind tunnel experiments, an estimate of wind speeds required for particle motion on Mars has been made and is currently in press. These results indicate that wind speeds on the order of 50 to 100 meters per second are required under optimum conditions on Mars. An analysis was also made of the Corioles effect which indicates that there would be a deviation of planetary winds from the surface of between 10 and 30 degrees, depending upon the latitude. Additional studies to determine the aerodynamic flow field around a crater's raised rim have resulted in a refinement of the general model and the derivation of computer programs to simulate the particle trajectories for particles moving past crater-shaped objects. Results of this study were published as a NASA Technical Memorandum (White et al., 1975).

3) Comparative Study of Basaltic Analogs to Lunar and Martian Volcanic Features. This phase of the investigation has involved preliminary geologic mapping of a 7½ minute quadrangle in the Snake River Plain of Idaho. This quadrangle covers a fissure and a series of vents over several rift zones in the Snake River Plain. Preliminary geologic mapping has been completed and awaits field studies. This work is being done in collaboration with Dr. Jack King, University of New York at Buffalo.

4) Geologic Field Studies of Maar Craters in the Snake River Plain. An investigation of Split Butte maar crater has been completed and the results published in a Geological Society of America Field Guide (Greeley and King, 1975). This crater is about 600 meters in diameter and has a complex geologic history involving initial eruptions of tephra, followed by the emplacement of a lava lake, subsidence of the lake to form a pit crater, and the intrusion of basaltic dikes through the tephra rim. Subsequent encroachment of the crater ring by younger basalt flows has produced a distinctive morphology which appears to be analogous to smaller structures in martian volcanic plains and to small ring-moat structures in certain mare plains of the Moon. An analysis of Sand Crater and China Cap Crater in the Snake River Plain is currently underway to serve as a comparison for Split Butte as well as the terrestrial features.

The above items summarize the work performed during the last six month period. The work for the initial six months on the grant is discussed in the Semi-Annual Progress Report, submitted in March, 1975.

A. Publications:

1. Ronald Greeley and Michael H. Carr, eds. A Geological Basis for the Exploration of the Planets. Review Copy, June 1975; to be NASA SP.

2. L. Colin, L. C. Evans, R. Greeley, W. L. Quaide, R. W. Schaupp, A. Seiff, R. E. Young. The Future Exploration of Venus (Post-Pioneer Venus 1978). NASA TM X-62,450, 1975.

3. Ronald Greeley and John S. King. Geologic Field Guide to the Quaternary Volcanics of the South-Central Snake River Plain, Idaho. Idaho Bureau of Mines and Geology, Moscow, Idaho. Pamphlet No. 160, 1975.

4. B. R. White, J. D. Iversen, R. Greeley, J. B. Pollack. Particle Motion in Atmospheric Boundary Layers of Mars and Earth. NASA TM X-62,463, 1975.

5. J. B. Pollack, R. Haberle, R. Greeley, J. Iversen. Estimates of the Wind Speeds Required for Particle Motion on Mars. MS, 1975.

6. Ronald Greeley. A Model for the Emplacement of Lunar Basin-Filling Basalts. Sixth Lunar Science Confr, p. 309-310, 1975.

7. Ronald Greeley, Ed. Hawaiian Planetology Conference Guidebook. NASA TM X 62,362, 1974.

8. R. Greeley, J. D. Iversen, B. White and J. Pollack. Aeolian Erosion on Mars. Geol. Soc. of Amer., vol. 6, no. 7, 1974.

THE FUTURE EXPLORATION OF VENUS (POST-PIONEER VENUS 1978)

L. Colin, L. C. Evans, R. Greeley, W. L. Quaide, R. W. Schaupp, A. Seiff and R. E. Young

NASA TM X-62,450

INTRODUCTION

This document attempts to summarize briefly the contents of an extensive report with the same title, to be published as NASA TM X-62,450, in July 1975. That report represents the culmination of a six-month (January-July 1975) in-house study, requested and supported by the Planetary Programs Office (Code SL) of the Office of Space Science (Code S) at NASA Headquarters. Some 30 research scientists and engineers participated in the study, all on a part-time basis. The scientists involved were drawn mainly from the Space Science Division. Those participants associated with mission and engineering aspects were drawn from the Systems Studies Division. As part of the study, a distinguished scientific board of review, intimately acquainted with planetary, and particularly, Venus exploration, was convened at Ames on June 12, 1975 to critically review our conclusions and recommendations. The report was modified considerably as a result of the constructive criticisms offered at that review. However, the final report should not be construed as an endorsement of our recommendations by the review board. The authors accept full responsibility for the entire contents therein.

The objectives of the study were to:

(1) Isolate the major scientific questions concerning the planet Venus that will remain following the Pioneer Venus missions ending in August 1979.

(2) Recommend a sequence of follow-on spacecraft missions to Venus for the 1980's.

(3) Recommend areas for early initiation of long lead-time experiment and instrument development, spacecraft engineering development, and mission analyses.

The study objectives were accomplished by addressing a logical sequence

of identifiable tasks:

(1) Outline the major goals of planetary exploration (origins, evolution, comparative planetology and meteorology). - (1.1)*

(2) Determine the role Venus exploration plays towards the fulfillment of those goals, and develop a comprehensive list of exploration objectives therefrom, appropriate to the Venus ionosphere, atmosphere, clouds, surface, and interior. - (1.2)

(3) Survey the current state-of-knowledge of Venus. - (3.0)

(4) Critically assess the contributions expected of (a) the Pioneer Venus Orbiter and Multiprobe Missions (1978-1979), (b) Earth-based radar and optical observations (1975-1980), and (c) potential Venera missions (1975, 1977, 1978) toward answering some of the outstanding, current scientific questions. - (4.0)

(5) Isolate the major limitations of the above programs and thereby the major gaps in knowledge which will exist in the post-Pioneer Venus time frame. - (5.0)

(6) Study the technological and instrumental feasibility, effectiveness, and uniqueness of particular spacecraft types [Orbiters (6.0), Entry Probes (7.0), Balloons and Dropsondes (8.0), Survivable Landers and Penetrators (9.0)] for addressing those major gaps in knowledge.

(7) Develop an optimum strategy for a sequence of spacecraft missions to Venus during the 1980's. - (10.0)

(8) Identify the major technological and instrumental developments required to support the implementation of our recommendations. - (10.0)

---

*Numbers in parens. are indicative of sections of the complete report

GEOLOGIC FIELD GUIDE
TO THE
QUATERNARY VOLCANICS OF THE
SOUTH-CENTRAL SNAKE RIVER PLAIN, IDAHO

RONALD GREELEY and JOHN S. KING

University of Santa Clara
NASA-Ames Research Center
Moffett Field, CA 94035

Dept. of Geological Sciences
State University of New York
Buffalo, NY 14207

ABSTRACT

Quaternary volcanic landforms of the south central Snake River Plain are described and discussed in a broad regional and structural framework of the Snake River Plain province. Specific volcanic features at King's Bowl near Crystal Ice Cave are documented and a detailed description and reconstructed geologic history of Split Butte, a maar crater is provided. The morphology of Split Butte is compared and contrasted with Sand Crater and China Cap, two other volcanic constructs in the same region. A discussion of lava tubes is presented and brief comparisons between Snake River Plain features and analogous extraterrestrial volcanic and impact phenomena is considered. A detailed road log for the trip from American Falls to Split Butte and the Crystal Ice Cave—King's Bowl area is included.

A Field Guide Prepared for the

28th Annual Meeting of the Geological Society of America

Rocky Mountain Section

Boise, Idaho

May, 1975

1. Report No.	2. Government Accession No.	3. Recipient's Catalog No.
TM X-62,463		

4. Title and Subtitle

PARTICLE MOTION IN ATMOSPHERIC BOUNDARY LAYERS OF MARS AND EARTH

5. Report Date

6. Performing Organization Code

7. Author(s)

Bruce R. White,[1] James D. Iversen,[2]
Ronald Greeley,[3] and James B. Pollack[4]

9. Performing Organization Name and Address

[1]University of California, Davis, CA 95616
[2]Iowa State University, Ames, Iowa 50010
[3]University of Santa Clara and Ames Research Center, NASA, Moffett Field, CA 94035
[4]Ames Research Center, NASA, Moffett Field, CA 94035

8. Performing Organization Report No.

A-6210

10. Work Unit No.

384-50-60

11. Contract or Grant No.

12. Sponsoring Agency Name and Address

National Aeronautics and Space Administration
Washington, D.C. 20546

13. Type of Report and Period Covered

Technical Memorandum

14. Sponsoring Agency Code

15. Supplementary Notes

16. Abstract In view of recent imagery received from the Mariner 9 spacecraft showing evidence of variable surface features and surface erosion resulting from atmospheric winds, a renewed interest has occurred in the eolian mechanics of saltating particles. To study this phenomenon both an experimental investigation of the flow field around a model crater in an atmospheric boundary layer wind tunnel and numerical solutions of the two- and three-dimensional equations of motion of a single particle under the influence of a turbulent boundary layer were conducted. Two-dimensional particle motion was calculated for flow near the surfaces of both Earth and Mars. For the case of Earth both a turbulent boundary layer with a viscous laminar sublayer and one without were calculated. For the case of Mars it was only necessary to calculate turbulent boundary layer flow with a laminar sublayer because of the low values of friction Reynolds number; however, it was necessary to include the effects of slip flow on a particle caused by the rarefied Martian atmosphere. In the equations of motion the lift force functions were developed to act on a single particle only in the laminar sublayer or a corresponding small region [illegible] near near the surface for a fully turbulent boundary layer. The lift force functions were [illegible] from the analytical work by Saffman concerning the lift force acting on a particle in simple [illegible] flow.

The numerical solutions for Earth were used to develop an approximate solution for the transition region and were empirically adjusted to agree with the experimental data. These modified equations were then solved to estimate particle motion under Mars surface conditions. These calculations show the importance of a lift force used in both Mars and Earth calculations.

Major findings include a comparison between Earth and Mars particle trajectories for equal ratios of friction to threshold friction speeds that shows Mars length scales in trajectories to be larger and with higher terminal particle velocities with lower collision angles at the surface than Earth's. Other significant results include simulated particle flow in the wake of a crater with a horseshoe vortex that shows extremely high terminal velocities and smaller than normal collision angles, especially for smaller particles, resulting in high erosion rates at the surface. Further, turbulence was shown not to play a major role in shaping particle trajectories, except for small particles. Also, particle rebound resulting from an inelastic collision at the Martian surface was calculated and showed increasing trajectory lengths for increasing momentum retained upon collision.

17. Key Words (Suggested by Author(s))	18. Distribution Statement
Planetary boundary layer Grain saltation Flow around crater	Unlimited

ESTIMATES OF THE WIND SPEEDS REQUIRED FOR PARTICLE MOTION ON MARS

J. B. Pollack, R. Haberle, R. Greeley, J. D. Iversen

Abstract

We have obtained estimates of the threshold wind speed V_{gt} near the top of the atmospheric boundary layer on Mars and of the rotation angle α between this wind velocity and the direction of the surface stress. This calculation has been accomplished by combining wind tunnel determinations of the friction velocity with semi-empirical theories of the Earth's atmospheric boundary layer. Calculations have been performed for a variety of values of the surface pressure, ground temperature, roughness height, boundary layer height, atmospheric composition, atmospheric stability, particle density, particle diameter, and strength of the cohesive force between the particles.

The curve of threshold wind speed as a function of particle diameter monotonically decreases with decreasing particle diameter for a cohesionless soil but has the classical "U" shape for a soil with cohesion. Observational data indicate that the latter condition holds on Mars.

Under "favorable" conditions minimum threshold wind speeds between about 50 and 100 m/s are required to cause particle motion. These minimum values lie close to the highest wind speeds predicted by general circulation models. Hence, particle motion should be an infrequent occurrence and should be strongly correlated with nearness to small topographic features. The latter prediction is in accord with the correlation found between albedo markings and topographic obstacles such as craters. For equal wind speeds at the top of the boundary layer, particle movement occurs more readily in general at night than during the day, more readily in the winter polar areas than the equatorial areas near noon, and more readily for ice particles than for silicate particles.

The boundary between saltating and suspendable particles is located at a particle diameter of about 100 microns. This value is close to the diameter at which the V_{gt} curve has its minimum. Hence, the wind can set directly into motion both saltating and larger sized suspendable particles, but dust storm sized particles usually require impact by a saltating particle for motion to be initiated. Albedo changes occur most often in regions containing a mixture of dust storm sized particles and saltating particles.

The threshold wind speed for surfaces containing large, nonerodible roughness elements can either be smaller or larger than the value for surfaces with only erodible material. The former condition for V_{gt} holds when the roughness height z_o is less than about 1 cm and may be illustrated by craters that have experienced less erosion than their environs. The latter condition for V_{gt} may be partly responsible for albedo changes detected on the elevated shield volcano, Pavonis Mons.

Values of the angle α generally lie between 10° and 30°. These figures place a modest limitation on the utility of surface albedo streaks as wind direction indicators.

Sixth Lunar Science Conf., 1975, pp. 309-310.

A MODEL FOR THE EMPLACEMENT OF LUNAR BASIN-FILLING BASALTS,

Ronald Greeley, Univ. Santa Clara, Ames Research Center, Mail Stop 245-5, Moffett Field, CA 94035

Despite extensive photographic, petrographic, and geophysical data, general models are lacking to explain the differences exhibited among mare units and their mode of emplacement. It is proposed that analyses of mare surface features and structure can explain these differences and, through terrestrial analogy, suggest specific modes of emplacement.

Because mare units are essentially basaltic, the presence or absence of certain types of surface features should signal chemical and physical conditions of the flow at the time of formation, just as they do terrestrially. Among the important parameters that determine the character of basalt flows are: 1) nature of the magma reservoir, 2) volume and frequency of eruption, 3) physical and chemical properties of the lava, 4) size, shape, and arrangement of the vent or vents, and 5) topography of the pre-flow surface. Differences in these parameters lead to at least three diverse basaltic terrains, each having a distinctive geomorphology: 1) flood-basalts, 2) basaltic shields, and 3) an intermediate terrain, informally termed here basaltic plains. Basaltic shields (e.g., Mauna Loa) characteristically are dominated by summit calderas and radial rift zones with smaller scale surface features such as cinder cones, spatter cones, lava tubes, and channels. Shields are constructional features built of relatively thin flows extruded by frequent (but nonetheless intermittent) eruptions which suggests a "leaky" magma reservoir (Swanson et al., 1974) in, perhaps, a constant state of production. There do not appear to be obvious lunar analogs to large shield volcanoes of dimensions comparable to the classic Hawaiian shields.

In contrast to shield-forming eruptions, the emplacement of flood basalts (e.g., the Columbia Plateau) involved super fissures that infrequently erupted large volumes (in some cases, three or four orders of magnitude higher than Hawaiian rates) of lava, perhaps from large lower crustal or upper mantle reservoirs (Swanson et al., 1974). Hundreds of square kilometers were inundated by flood basalts, many of which were "ponded" to great depth. Nearly all large surface flow features were obliterated (if any formed in the first place), as were most of the vent structures, which resulted in large, fairly flat and nearly featureless surfaces. In cross section, flood basalts exhibit typical colonade-entablature joint and fracture patterns. The lunar counterpart to flood basalts is suggested to be the emplacement of most Imbrian age basin-filling basalts and some Eratosthenian units, such as those of Mare Crisium. These units, in general, have a relative abundance of mare ridges, but lack well defined and extensive flow features such as sinuous rilles. At least some mare ridges may represent large-scale crustal buckling of ponded flows.

Basaltic plains (e.g., Snake River Plain, Idaho) are intermediate between flood basalts and shields in their characteristics. Basaltic plains are built

EMPLACEMENT OF LUNAR BASALTS

Greeley, R.

of numerous small, very low profile lava cones (small, low-relief shields) that coalesce and overlap one another. The cones are composed of multiple thin flows erupted from small (~ 1 km in diameter and less) vents; flow features such as lava tubes and channels are common. In this respect, basaltic plains are similar to shields, but rather than forming large constructional mountains from centralized vents, the vents in basaltic plains are distributed over a wide area.

Lunar analogs for terrestrial basaltic plains are suggested to be many Eratosthenian mare basalts, typified by the Imbrium lava flows and others. These are clearly very thin units which appear to overlie more massive Imbr flows. Most generally accepted lunar volcanic surface features, such as sinuous rilles, domes, cones, and other vent areas, etc., occur in Eratosthenian flows, or are closely associated with them. By terrestrial analogy, these features are characteristic of basaltic plains rather than flood basalts, which suggests intermittent eruptions of relatively lower volume lavas.

Preliminary analyses of the type and distribution of lunar surface features in space and time suggests that basins were initially filled with flood-type basalts which left few, if any, vestiges of source vents or flow features. Lavas were probably ponded to depths in excess of 100 m and as cooling and degassing progressed, subsidence left high lava benches and produced some mare ridges. This stage was followed by relatively sporadic and intermittent eruptions (whose eruptive centers were at least partly preserved) that produced sinuous rilles, collapse depressions, and some additional mare ridges. These lavas could represent newly generated magma reservoirs, or could be the extrusion of still-molten lava from beneath the crust of the earlier-formed lava ponds.

Lack of identifiable flow features in some lunar basins, such as Mare Crisium, suggests that the second stage eruptions did not occur, or were weakly developed.

References Cited

Swanson, D. A., T. L. Wright, and R. T. Helz, 1974. Linear vent systems and estimated rates of magma production and eruption for the Yakima Basalt. Presented at the Hawaiian Planetology Conference, Hilo, Hawaii, Oct., 1974.

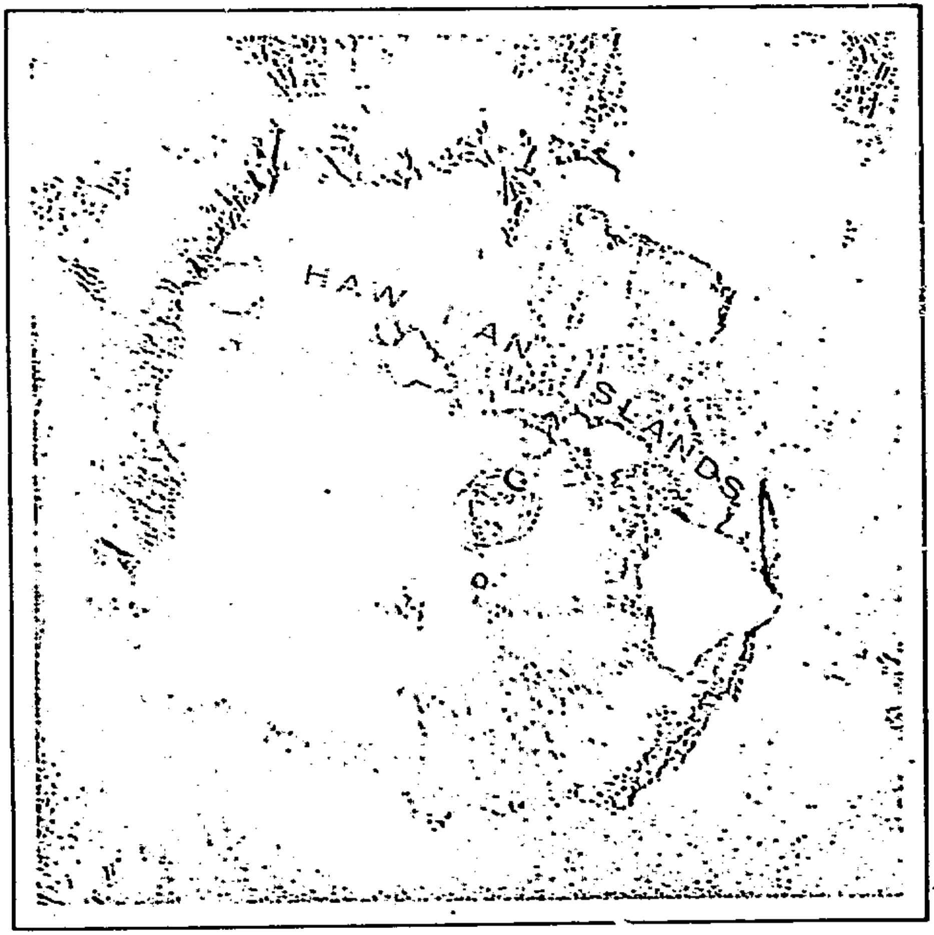

HAWAIIAN PLANETOLOGY CONFERENCE

Ronald Greeley
Editor

NASA/Ames Research Center

University of Santa Clara, California, Hawaiian Volcano Observatory–United States Geological Survey, Hawaii

NASA TMX 62362 prepared for the Mars Geologic Mapping Meeting, sponsored by the Office of Planetology Programs, National Aeronautics and Space Administration, Washington, D.C.

AEOLIAN EROSION ON MARS PART I: EROSION RATE SIMILITUDE

Iversen, James D., Iowa State University, Ames, Ia. 50010; Greeley, Ronald, Physics Department, University of Santa Clara, Ca. 95053; White, Bruce, Iowa State University, Ames, Ia. 50010; Pollack, James B., NASA-Ames Research Center, Moffett Field, Ca. 94035

In Part One of this set of two papers, an erosion rate similitude parameter is derived, which is based on theoretical considerations of erosion of wind-blown sand. This parameter is used to correlate wind tunnel experiments of particle motion over model craters. The characteristics of the flow field in the vicinity and downwind of a crater are discussed. The existence of a trailing horseshoe vortex system is illustrated by comparison of photographs of time-dependent erosion caused by (1) model craters and (2) the trailing vortex system from a model wing.

The erosion rate correlation equation is

$$A/A_c = K_o(u_F/u_{*t})\ (\rho/\rho_p)\ (u_{*t}^2/gD_c)(u_*/u_{*t})\ (K_1\ (u_*/u_{*t})\ -1)\ (u_{*t}\ \Delta t/h)$$

where u_F is particle terminal speed, u_{*t} is threshold friction speed, ρ is air density, ρ_p is particle density, g is gravitational acceleration, D_c is crater diameter, u_* is friction speed, Δt is time, h is mean eroded depth, A is eroded surface area, [illegible] and K_o and K_1 are coefficients which are functions of [illegible]. The correlation equation is shown to effectively correlate data from a series of tests incorporating a range of values of the important modeling parameters by variation of surface material density and diameter, model crater diameter, and wind speed. Estimates of erosion [illegible] calculated from the equation are presented in Part II.

AEOLIAN EROSION ON MARS PART II: ESTIMATED THICKNESS OF SURFACE DUST IN THE DAEDALIA REGION OF MARS, 1971

Greeley, Ronald, Physics Department, University of Santa Clara, Ca. 95053; Iversen, James D., Iowa State University, Ames, Ia. 50010; White, Bruce, Iowa State University, Ames, Ia. 50010; Pollack, James B., NASA-Ames Research Center, Moffett Field, Ca. 94035

Results from the Mariner 9 mission to Mars show numerous areas containing "variable" features, i.e., surface patterns that changed temporally. Most of the variable features are associated with topographic obstructions (usually craters) and it is generally believed that they are aeolian in origin. At least some dark fans associated with craters represent surfaces that have been swept free of particles by the wind in the turbulent zone of the crater wake (Greeley et al., 1974). Using the general erosion rate parameter derived above (Part I), estimates were made for the depth of particles assumed to have been swept free in the wake of craters in the Daedalia Region of Mars (approximately 28°S latitude, 122.5°W longitude) during a 38 day period in 1971 (Mariner images DAS 05707278 and 05585264). Based on the following estimated martian conditions: friction velocity = 310 cm/sec, threshold velocity = 207 cm/sec, ratio of atmospheric density to particle density = 3.978×10^{-6}, surface pressure of 5 mb, and a nominal crater rim height to diameter ratio of 0.1, the depth of aeolian particles removed by the wind averaged 2.4 mm for 17 cases examined in the region. This value is based on calculations assuming grain size that is optimum for aeolian movement on Mars (100μ), and assuming that the wind blew steadily during the 38 day interval.

ERI – 74194
PREPRINT
Project 1069

Engineering Research Institute

IOWA STATE UNIVERSITY
AMES

SALTATION THRESHOLD ON MARS; THE EFFECT OF INTERPARTICLE FORCE, SURFACE ROUGHNESS, AND LOW ATMOSPHERIC DENSITY

ABSTRACT

The effect of interparticle forces, as well as changes in surface roughness, particle diameter and density, and atmospheric density and viscosity are considered in new estimates of saltation threshold on Mars. These estimates result in somewhat lower minimum values of predicted threshold speed than have been previously reported, with the minimum threshold speed occuring at smaller values of particle diameter. It is shown that the new predictions are much closer to the limited low atmospheric density data available than if the older method of estimation is used.

This paper was prepared for submission to
Icarus

23 pages, 7 figures

ERI – 74195
PREPRINT
Project 1069

Engineering Research Institute

IOWA STATE UNIVERSITY

AMES

EOLIAN EROSION ON THE MARTIAN SURFACE;

PART 1: EROSION RATE SIMILITUDE

J. D. Iversen*, R. Greeley**, B. R. White***, J. B. Pollack****

ABSTRACT

A similitude parameter is derived which is based on theoretical considerations of erosion due to sand in saltation. This parameter has been used to correlate wind tunnel experiments of particle flow over model craters. The characteristics of the flow field in the vicinity and downstream of a crater are discussed and it is shown that erosion is initiated in areas lying under a pair of trailing vortices. The erosion rate parameter is used to calculate erosion rates on Mars, reported in Part 2, to be published later.

This paper was prepared for submission to
Icarus

14 pages, 10 figures, 2 tables

Submitted for publication

MARS: ESTIMATED THICKNESS OF MOBILE DUST IN DAEDALIA

Ronald Greeley[1]

James D. Iversen[2]

James B. Pollack[3]

Abstract

Thickness of the dust layer on the ground in the Daedalia region of Mars during the 1971 dust storm averaged 0.7 mm in the vicinity of craters. This estimate is based on an erosion rate similitude parameter that was derived from wind tunnel experiments.

[1]Department of Physics, University of Santa Clara, CA 95053
Mail address: NASA-Ames Research Center, Mail Stop 245-5, Moffett Field, CA 94035

[2]Department of Aerospace Engineering, Iowa State University, Ames, Iowa 50010

[3]Space Sciences Division, NASA-Ames Research Center, Moffett Field, CA 94035

C. DR. CURTIS W. PARKIN: Lunar Magnetism.

Magnetic field data from three Apollo lunar surface magnetometers and from lunar orbiting magnetometers have been analyzed to investigate properties of the lunar interior and the lunar environment. Results have been published or submitted for publication in the following specific areas of research: (1) global electrical conductivity and temperature of the moon, (2) lunar magnetic permeability, (3) iron abundance of the moon, and (4) properties of the lunar ionosphere. Publications and verbal presentations for the time period September 1, 1974 - August 31, 1975 are listed below. Abstracts are included in the Appendix.

A. Publications:

1. P. Dyal, C. W. Parkin, and W. D. Daily, "Magnetism and the Interior of the Moon," Rev. Geophys. Space Phys. 12, 568, 1974.

2. C. W. Parkin, W. D. Daily, and P. Dyal, "Iron Abundance and Magnetic Permeability of the Moon," Proc. Fifth Lunar Sci. Conf., Geochim. Cosmochim. Acta, vol. 3, pp. 2761-2778, 1974.

3. P. Dyal, C. W. Parkin, and W. D. Daily, "Temperature and Electrical Conductivity of the Lunar Interior from Magnetic Transient Measurements in the Geomagnetic Tail," Proc. Fifth Lunar Sci. Conf., Geochim. Cosmochim. Acta, vol. 3, pp. 3059-3071, 1974.

4. P. Dyal, C. W. Parkin, and W. D. Daily, "Lunar Electrical Conductivity and Magnetic Permeability," Proc. Sixth Lunar Sci. Conf., Geochim. Cosmochim. Acta, vol. 3, 1975, in press.

B. Verbal Presentations:

1. P. Dyal, C. W. Parkin, and W. D. Daily, "Global Lunar Properties from Surface Magnetometer Measurements," in Lunar Science VI, p. 226, Sixth Lunar Science Conference, Houston, Texas, March 1975.

2. C. W. Parkin, W. D. Daily, and P. Dyal, "Relative Magnetic Permeability and Iron Abundance of the Moon," presented at the 56th Annual Meeting, American Geophysical Union, Washington, D.C., June, 1975.

3. W. D. Daily, W. A. Barker, P. Dyal, and C. W. Parkin, "A Model Lunar Ionosphere for the Moon in the Geomagnetic Tail," presented at the 56th Annual Meeting, American Geophysical Union, Washington, D.C., June, 1975.

VOL. 12, NO. 4 REVIEWS OF GEOPHYSICS AND SPACE PHYSICS NOVEMBER 1974

Magnetism and the Interior of the Moon

PALMER DYAL

NASA Ames Research Center, Moffett Field, California 94035

CURTIS W. PARKIN

Department of Physics, University of Santa Clara, Santa Clara, California 95053

WILLIAM D. DAILY

Department of Physics and Astronomy, Brigham Young University, Provo, Utah 84602

During the time period 1961–1972, 11 magnetometers were sent to the moon. The primary purpose of this paper is to review the results of lunar magnetometer data analysis, with emphasis on the lunar interior. Magnetic fields have been measured on the lunar surface at the Apollo 12, 14, 15, and 16 landing sites. The remanent field values at these sites are 38, 103 (maximum), 3, and 327 γ (maximum), respectively. Simultaneous magnetic field and solar plasma pressure measurements show that the Apollo 12 and 16 remanent fields are compressed during times of high plasma dynamic pressure. Apollo 15 and 16 subsatellite magnetometers have mapped in detail the fields above portions of the lunar surface and have placed an upper limit of 4.4×10^{18} G cm^3 on the global permanent dipole moment. Satellite and surface measurements show strong evidence that the lunar crust is magnetized over much of the lunar globe. Magnetic fields are stronger in highland regions than in mare regions and stronger on the lunar far side than on the near side. The largest magnetic anomaly measured to date is between the craters Van de Graaff and Aitken on the lunar far side. The origin of the lunar remanent field is not yet satisfactorily understood; several source models are presented. Simultaneous data from the Apollo 12 lunar surface magnetometer and the Explorer 35 Ames magnetometer are used to construct a whole moon hysteresis curve from which the global lunar permeability is determined to be $\mu = 1.012 \pm 0.006$. The corresponding global induced dipole moment is $\sim 2 \times 10^{18}$ G cm^3 for typical inducing fields of 10^{-4} G in the lunar environment. From the permeability measurement, lunar free iron abundance is determined to be 2.5 ± 2.0 wt %. Total iron abundance (sum of iron in the ferromagnetic and paramagnetic states) is calculated for two assumed compositional models of the lunar interior. For a free iron/orthopyroxene lunar composition the total iron content is 12.8 ± 1.0 wt %; for a free iron/olivine composition, total iron content is 5.5 ± 1.2 wt %. Other lunar models with a small iron core and with a shallow iron-rich layer are also discussed in light of the measured global permeability. Global eddy current fields, induced by changes in the magnetic field external to the moon, have been analyzed to calculate lunar electrical conductivity profiles by using several different analytical techniques. From night side transient data, ranges of conductivity profiles have been calculated. At a depth of 250 km into the moon, the conductivity ranges between 1×10^{-4} and 2×10^{-3} mhos/m. Thereafter, conductivity rises with depth and ranges between 2×10^{-3} and 8×10^{-2} mhos/m at 1000 km depth. Harmonic analyses of day side data are similar to night side results except at the greater lunar depths, where harmonic day side profiles show lower conductivities than the night side results do. Transient response analysis has recently been applied to data measured in the lobes of the geomagnetic tail, and thus calculation is allowed of a conductivity profile that increases with depth from 10^{-9} mho/m at the lunar surface to 10^{-4} mho/m at 200 km depth then to 2×10^{-2} mho/m at 1000 km depth. This profile is generally consistent with conductivity results from transient response analysis in the solar wind, in which data measured on the lunar night side are used. A temperature profile is calculated from this conductivity profile by using the data of Duba et al. (1974); temperature rises rapidly with depth to 1100°K at 200 km depth then less rapidly to 1800°K at 1000 km depth.

Proceedings of the Fifth Lunar Conference
(Supplement 5, Geochimica et Cosmochimica Acta)
Vol. 3 pp. 2761–2778 (1974)
Printed in the United States of America

Iron abundance and magnetic permeability of the moon

CURTIS W. PARKIN
Department of Physics, University of Santa Clara, Santa Clara, California 95053

WILLIAM D. DAILY
Department of Physics and Astronomy, Brigham Young University, Provo, Utah 84602

PALMER DYAL
NASA Ames Research Center, Moffett Field, California 94035

Abstract—A larger set of simultaneous data from the Apollo 12 lunar surface magnetometer and the Explorer 35 Ames magnetometer are used to construct a whole-moon hysteresis curve, from which a new value of global lunar permeability is determined to be $\mu = 1.012 \pm 0.006$. The corresponding global induced dipole moment is 2.1×10^{18} gauss-cm^3 for typical inducing fields of 10^{-4} gauss in the lunar environment. From the permeability measurement, lunar free iron abundance is determined to be 2.5 ± 2.0 wt.%. Total iron abundance (sum of iron in the ferromagnetic and paramagnetic states) is calculated for two assumed compositional models of the lunar interior: a free iron/orthopyroxene lunar composition and a free iron/olivine composition. The overall lunar total iron abundance is determined to be 9.0 ± 4.7 wt.%. Other lunar models with a small iron core and with a shallow iron-rich layer are discussed in light of the measured global permeability. Effects on permeability and iron content calculations due to a possible lunar ionosphere are also considered.

Proceedings of the Fifth Lunar Conference
(Supplement 5, Geochimica et Cosmochimica Acta)
Vol. 3 pp. 3059–3071 (1974)
Printed in the United States of America

Temperature and electrical conductivity of the lunar interior from magnetic transient measurements in the geomagnetic tail

PALMER DYAL

NASA Ames Research Center, Moffett Field, California 94035

CURTIS W. PARKIN

Department of Physics, University of Santa Clara, Santa Clara, California 95053

WILLIAM D. DAILY

Department of Physics and Astronomy, Brigham Young University, Provo, Utah 84062

Abstract—Magnetometers have been deployed at four Apollo sites on the moon to measure remanent and induced lunar magnetic fields. Global lunar fields due to eddy currents, induced in the lunar interior by magnetic transients, have been analyzed for the first time within the lobes of the geomagnetic tail field. An electrical conductivity profile has been calculated for the moon: the conductivity increases rapidly with depth from 10^{-9} mhos/m at the lunar surface to 10^{-4} mhos/m at 200 km depth, then less rapidly to 2×10^{-2} mhos/m at 1000 km depth. This profile is generally consistent with conductivity results from transient response analysis in the solar wind, using data measured on the lunar nightside. A temperature profile is calculated from conductivity, using the data of Duba *et al.* (1974): Temperature rises rapidly with depth to 1100°K at 200 km depth, then less rapidly to 1800°K at 1000 km depth. Velocities and thicknesses of the earth's magnetopause and bow shock at the lunar orbit are estimated from simultaneous magnetometer measurements. Average speeds are determined to be about 50 km/sec for the magnetopause and 70 km/sec for the bow shock, although there are large variations in the measurements for any particular boundary crossing. Corresponding measured boundary thicknesses average to about 2300 km for the magnetopause and 1400 km for the bow shock at the position of the lunar orbit.

Proceedings of the Sixth Lunar Science Conference, Geochim. Cosmochim. Acta, Suppl. 6, vol. 3, 1975, in press.

LUNAR ELECTRICAL CONDUCTIVITY AND MAGNETIC PERMEABILITY

Palmer Dyal
NASA-Ames Research Center, Moffett Field, California 94035

Curtis W. Parkin
Department of Physics, University of Santa Clara
Santa Clara, California 95053

William D. Daily
Department of Physics and Astronomy
Brigham Young University, Provo, Utah 84602

Abstract--Improved analytical techniques are applied to a larger Apollo magnetometer data set to yield values of electrical conductivity, temperature, magnetic permeability, and iron abundance. Average bulk electrical conductivity of the moon is calculated to be 7×10^{-4} mho/m. Allowable solutions for electrical conductivity indicate a rapid increase with depth to $\sim 10^{-3}$ mho/m within 250 km. The upper limit on the calculated size of a hypothetical highly conducting core ($\geq 7 \times 10^{-3}$ mho/m) is 0.57 R/R_{moon}. The temperature profile obtained from the electrical conductivity profile using the laboratory data of Duba et al. (1974) for olivine, indicates high lunar temperatures at relatively shallow depths. These results imply that the Curie isotherm is at a depth of less than 200 km. Magnetic permeability of the moon relative to its environment is calculated to be 1.008 ± 0.005. Adjustment of this result to account for a diamagnetic lunar ionosphere yields a lunar permeability, relative to free space, of $1.012^{+0.011}_{-0.008}$. Lunar iron abundances corresponding to this permeability value are $2.5^{+2.3}_{-1.7}$ wt.% free iron, and 5.0 to 13.5 wt.% total iron for a moon composed of a combination of free iron, olivine, and orthopyroxene.

GLOBAL LUNAR PROPERTIES FROM SURFACE MAGNETOMETER MEASUREMENTS,

P. Dyal*, C.W. Parkin**, and W.D. Daily***.
*NASA-Ames Research Center, Moffett Field, CA 94035
**Univ. of Santa Clara, Santa Clara, CA 95053
***Brigham Young Univ., Provo, Utah 84601

Data from the Apollo 12, 15, and 16 magnetometer network have been used to calculate the internal electrical conductivity profile and magnetic permeability of the moon. Model calculations have been carried out to determine the effect of a lunar ionosphere on permeability results. A thermoelectric current model for the ancient source of the remanent magnetic fields has also been examined.

Lunar electrical conductivity results have been determined using a new analytical technique. A superposition of electromagnetic transient events, each in three orthogonal axes, is obtained from two-hour sets of simultaneous Apollo and Explorer magnetometer data. The total data set is ten times larger than previously used and allows deeper sounding of the lunar interior. This new technique yields an improved profile and permits the size and conductivity of model lunar cores to be studied.

A new technique has also been developed for calculating the relative magnetic permeability and iron abundance of the moon which involves the use of simultaneous surface magnetometer measurements only, and does not depend upon orbital data. The high resolution of the Apollo surface instruments, their proximity to the permeable lunar globe, and the simultaneous use of three orthogonal vector components permit a more accurate determination of the interior iron abundance. A model for the lunar ionosphere in the geomagnetic tail has been examined for effects on the lunar permeability determination. This model assumes that upon entering the geomagnetic tail the moon quickly loses its lighter atmospheric constituents by thermal escape, leaving principally argon and neon to be photoionized. Consideration of the ionization process suggests that argon and neon are ionized and exist at approximately 300°K, and the electrons are at a temperature of 20 ev. It is these energetic electrons which dominate the ionospheric dynamics and are responsible for a rapid thermal loss of both ions and electrons. A lower limit of 0.9 is calculated for the permeability of this diamagnetic ionosphere.

Thermoelectric currents have been used in a model of the ancient source of the remanent fields measured by Apollo 12, 14, 15, and 16 magnetometers. In this model thermal gradients in cooling mare lavas produce Thomson thermoelectromotive forces which drive currents through the mare. The solar wind plasma, highly conducting along magnetic field lines, conducts the electrical current from the top surface of the lava to the lunar surface outside the mare; the lunar interior completes the circuit. Preliminary calculations show that under certain conditions, field strengths up to 500 gammas are possible.

RELATIVE MAGNETIC PERMEABILITY AND IRON ABUNDANCE OF THE MOON

C.W. Parkin (Dept. of Physics, U. of Santa Clara, Santa Clara, California 95053)
W.D. Daily (Dept. of Physics and Astronomy, Brigham Young U., Provo, Utah 84602)
P. Dyal (Space Science Div., NASA-Ames Research Center, Moffett Field, California 94035)

The relative magnetic permeability of the moon has been calculated using a new technique which employs simultaneous Apollo 15 and Apollo 16 lunar surface magnetometer data and requires no orbital magnetometer data. This method has the advantages of (1) higher resolution of the surface magnetometers and (2) results are not sensitive to instrument zero offsets. Data are selected from deep geomagnetic tail lobes where plasma effects are minimized, and ten-minute averages of steady data are used so that eddy current induction effects are negligible. The result is a value of $\mu = 1.008 \pm 0.005$ for the bulk relative permeability of the moon. To determine the absolute lunar permeability and iron abundance in the moon, we must consider the magnetic permeability of the environment exterior to the moon, in particular, that of the lunar ionosphere in the geomagnetic tail. We have determined theoretically a value of $\mu_i \cong 0.80$ for the lunar ionosphere; using this value we calculate an absolute bulk magnetic permeability best value of $\mu_m = 1.012$ for the moon. Iron abundance in the moon corresponding to magnetic permeability will be presented as a function of thermal profile and composition of the lunar interior. In particular for a temperature model with the Curie isotherm at 170 km depth, the best value of free iron abundance is 2.9 wt.%. Total iron abundance in the moon is calculated by adding free iron and combined iron abundances; the latter is dependent upon the material used to model the lunar interior. For a free iron/olivine model the total lunar iron abundance is 5.3 wt.%, and for a free iron/orthopyroxene moon the total iron abundance is 12.6 wt.%.

A MODEL LUNAR IONOSPHERE FOR THE MOON IN THE GEOMAGNETIC TAIL

W.D. Daily (Dept. of Physics and Astronomy, Brigham Young Univ., Provo, Utah 84602)
W.A. Barker (Dept. of Physics, U. of Santa Clara, Santa Clara, California 95053)
P. Dyal (Space Science Div., NASA-Ames Research Center, Moffett Field, California 94035)
C.W. Parkin (Dept. of Physics, U. of Santa Clara, Santa Clara, California 95053)

Previous models of the lunar ionosphere have been confined to times when the moon is in the solar wind. In this paper we describe a model lunar ionosphere for conditions when the moon is shielded from the solar wind by the geomagnetosphere. In the solar wind the lighter elements of He, H_2 and H are significant components of the lunar atmosphere. In addition, this atmosphere is ionized principally by charge exchange, and the motional electric field of the solar wind is responsible for the loss rate of the ionosphere from the moon. On the other hand, during the four days of each lunation when the moon is in the geomagnetic field, the He, H_2 and H thermally escape and do not contribute significantly to the atmosphere. Ne and Ar become the main atmospheric components. This atmosphere is photoionized, resulting in ions which are essentially in thermal equilibrium with the lunar surface (300°K); and electrons are calculated to have energies of approximately 20eV. These high energy electrons would escape very rapidly except that charge neutrality requires that they be restrained by the low energy ions. Theoretical results will be presented for scale height of the lunar ionosphere as a function of electron temperature and ion mass. An estimate is obtained for the mean lifetime of ions and electrons, and the ion density near the surface is calculated to be ~ 0.2 cm^{-3}. The ionosphere is a diamagnetic plasma and near 100 km altitude it is characterized by a magnetic permeability of ~ 0.8.

D. DR. HANS R. AGGARWAL: Martian and Lunar Cratering Studies.

During the period from March 1, 1975 to August 31, 1975, an investigation of the spacial distribution of the martian craters and a study of their morphology was carried out. The results of this work will be presented at two meetings - the International Colloquium of Planetary Geology to be held in September, 1975, in Rome and the Annual AGU meeting to be held in December, 1975, in San Francisco. Abstracts of the talks to be given at these meetings are enclosed for detailed information on the work accomplished.

A. Presentations

1. H. R. Aggarwal and V. R. Oberbeck. A Morphological Study of Martian Doublet Craters.

2. H. R. Aggarwal and V. R. Oberbeck. Spacial Distribution of Martian Craters.

A MORPHOLOGICAL STUDY OF MARTIAN DOUBLET CRATERS

By AGGARWAL, H. R.
Department of Physics, University of Santa Clara,
Santa Clara, CA 95053 U.S.A.

and OBERBECK, V. R.
Space Science Division, NASA-Ames Research Center,
Moffett Field, CA 94035 U.S.A.

This paper presents the results of a morphological study of martian doublet craters as revealed by the Mariner 9 photography. A study of the martian doublets based on the Mariner 6 and 7 photographs was previously carried out by Oberbeck and Oayagi (1972) who pointed out to the non-random distribution of these doublets. Their analysis led them to conclude that the martian doublets may have been produced by volcanic processes or by the fragments of weak bodies broken up by tidal fission before impacting. The present study differs from the above in that it considers a wider area, the whole $\pm 30°$ latitude equatorial belt, for its crater population and carries out a probability calculation for craters with diameters greater than or equal to 30 kilometers. The latter restriction is prescribed to take into account the possibility of obliteration which may erode smaller size class craters leaving clusters behind (Chapman 1974).

We have recorded 13,772 craters, noted their sizes, counted both kinds, tangential and intersecting types, of doublets occurring singly or as members of cluster craters, noted the structural features of the doublets like the presence or absence of septa between the member craters of a doublet, and taken a count of the craters with central peaks. A total of 1371 doublets were observed. Out of these, 477 doublets consisted of members of the same or almost of the same relative age (hereafter called SAS doublets), 126 of them having septa between their members. A percentage wise frequency-average diameter distribution of these doublets is shown in Fig. 1a and 1b. Fig. 1a shows an excessive production of SAS type doublets with septa over similar kind doublets having different age (DA) members, Fig. 1b shows a lack of DA type doublets of average diameters less than 30 kilometers. The scarcity of such doublets may be due to episodic obliteration or partially due to lack of secondaries reaching parts of the equatorial belt from basins on account of high gravity of Mars (Oberbeck et al 1975) and partially due to eolian and fluvian erosion (Chapman 1974). A percentage wise distribution of the doublets for varying ratio, r_{max}/r_{min}, of the member craters diameters, Fig. 2, shows that the members of a majority of SAS type doublets are nearly of the same size. A total of 417 craters with

with central peaks, 31 occurring in cluster craters, were counted. A classwise percentage with respect to the total number of craters in the class, Fig. 3, point to the preferred tendency of the central peaks to form in isolated craters.

Laboratory experiments (Oberbeck 1973) show that septa typically form when fragments impact far apart and central peaks form when fragments impact very near one another simultaneously producing one crater. The above evidence, namely, the excessive production of SAS type doublets, presence of septa, approximate equal size and age of member craters and the preferred tendency of the central peaks to form in isolated craters, lend their support to the conclusion reached previously that the martian doublets may have been produced by the non-random process of simultaneous impact. This conclusion was further confirmed by the probability calculation carried out for craters with diameters greater than or equal to 30 kilometers in the entire equatorial region of the CU terrain. The total population consists of some 1060 craters over an area of 30.5155×10^6 Km^2. The result of this calculation shows that 62 doublets may form under a random process. This number is much less than 138, the number of doublets actually observed in the CU terrain.

Our conclusions that there is a non-random clustering of craters greater than 30 Kms is quite consistent with similar recent observations of Trask et al 1975 that the heavily cratered terrain on Mercury consists of clusters of craters greater than 30 Kms in diameter. Trask et al 1975, Strom et al 1975 and Murray et al 1975 all note that the heavily cratered terrain on Mercury is younger than the intercrater terrain. This implies that at least some of the craters were produced in clusters on the older surface. Our preliminary observations suggest that the distribution of craters in the heavily cratered mercurian terrain is non-random spacially.

BIBLIOGRAPHY

Oberbeck, V. R. and M. Oayagi, "Martian Doublet Craters", J. Geophysical Res. Vol. 77, pp. 2419-2432, 1972.

Oberbeck, V. R., W. L. Quaide and R. E. Arvidson, "Secondary Cratering on Mercury, The Moon, and Mars", paper presented at the International Colloquium of Planetary Geology held at Rome, Sept. 22-30, 1975.

Chapman, C. R., "Cratering on Mars 1. Cratering and Obliteration History", Icarus, Vol. 22, pp. 272-291, 1974.

Oberbeck, V. R., "Simultaneous Impact and Lunar Craters", The Moon, Vol. 6, pp. 83-92, 1973.

Trask, N. J. and J. E. Guest, "Preliminary Geologic Terrain Map of Mercury", J. Geophysical Res. Vol. 80, pp. 2461-2477, 1975.

Strom, R. G., N. J. Trask and J. E. Guest, "Tectonism and

Volcanism of Mercury", J. Geophysical Res. Vol. 80, pp. 2478-2507, 1975.

Murray, B. C., R. G. Strom, N. J. Trask and D. E. Gault, "Surface History of Mercury: Implications for Terrestrial Planets", J. Geophysical Res. Vol. 80, pp. 2508-2514, 1975.

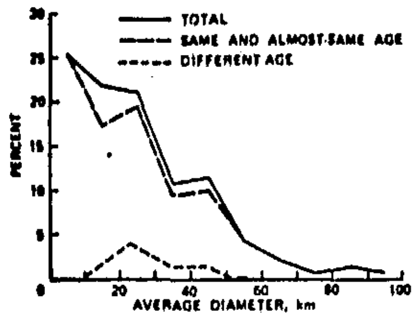

Fig. 1a. Percentage of doublets with septa at average diameter D.

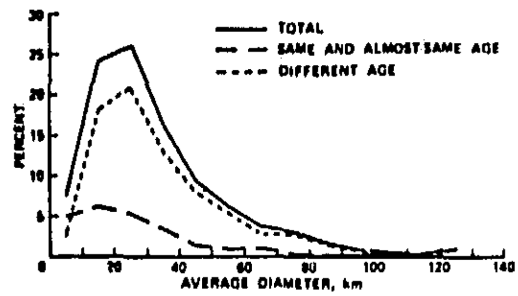

Fig. 1b. Percentage of doublets without septa at average diameter D.

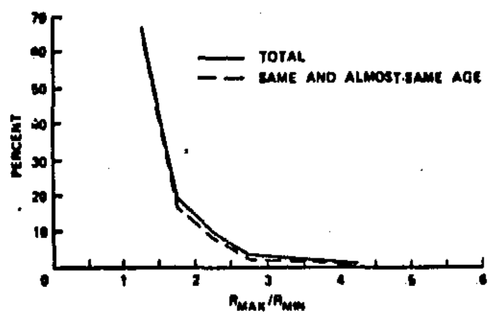

Fig. 2a. Percentage of doublets with septa versus diameter ratio.

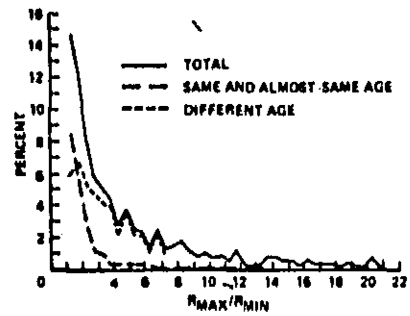

Fig. 2b. Percentage of doublets without septa versus diameter ratio.

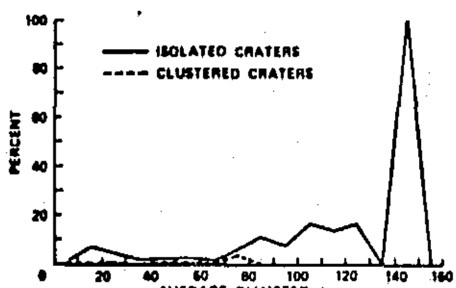

Fig. 3. Classwise percentage of central peak craters at average diameter D.

SPACIAL DISTRIBUTION OF MARTIAN CRATERS

H. R. Aggarwal (Dept. of Physics, Univ. of Santa Clara, Santa Clara, CA 95053)
V. R. Oberbeck (NASA-Ames Research Center, Moffett Field, CA 94035)
(Sponsor: J. F. Vedder)

Non-random spacial distribution of Martian craters has previously been reported in limited areas of the surface. While many of these craters occur in clusters, there is also a tendency of craters to occur in pairs. In this study, we report reults of a statistical and morphological analysis of craters in the equatorial zone ±30° of Mars. Only craters >30 km in diameter were considered. This was done to exclude the possibility that clustering is due to crater obliteration. We find evidence for non-randomness of craters: (a) doublets with septa have a tendency to have members of the same size and age. (b) probability calculations carried out for craters in the CU terrain show that whereas only 62 pairs should form from random single body impact, there are, in fact, 138 crater pairs observed. Although the distribution is non-random, many of the doublets could have been produced by simultaneous impact. Septa like those on the Mars doublets typically form between craters formed at the same time in the laboratory. A tendency for central peaks to form mostly in isolated craters rather than cluster members can also be understood if central peaks are due to fragments impacting very near one another at the same time on Mars since under these conditions, during laboratory impact tests, single craters with central peaks form. Clustering of craters may also occur on Mercury. Trask and Guest (JGR, vol. 80, 1975, p. 2469) have reported clusters of craters >30 km on the surface of Mercury. Our preliminary observations suggest that these craters like those on Mars are non-randomly distributed.

E. DR. PETER H. SCHULTZ: Degradation of Small Lunar Surface Features.

The following tasks were completed during the grant period (my participation being for six months):

(1) Seismic energy as a modifying agent. Theoretical and morphological studies of the possible magnitude of impact-generated shock and seismic waves have been made for craters ranging from 1 km to 600 km in diameter. Results suggest that massive surface disruption occurred diametrically opposite the major impact basins owing to shock waves travelling directly through the planet. Observational evidence for such a process includes distinctive hilly and lineated terrains recognized antipodal to the Imbrium and Orientale basins on the Moon and the Caloris basin on Mercury. Similarly, the formation of smaller size (100 km diameter) craters produced large shock pressures to 3-4 crater radii and may be responsible for (1) degradation of small craters and (2) degradation of the secondary and tertiary ejecta facies. These results were published in Schultz and Gault (1975a and 1975b).

(2) Degradation of primary surface features. Small surface features (50m-200m) associated with the emplacement of lunar mare basalts have been recognized and mapped in selected regions. The preservation of such small structures placed constraints of the rate and style of degradation over the last three billion years. Preliminary results suggest that the degradation of craters between 500m and 1 km must include not only long-term processes such as meteoritic erosion but also short-term processes such as seismically induced mass transfer and ejecta (impact and volcanic) blanketing. These results will be presented at the Fall Meeting of the American Geophysical Union.

(3) Crater Statistical Studies. Selection has been made of units and sites exhibiting different solar illuminations and surface strengths. Crater populations on these surfaces will be measured in the coming year.

A. Publications:

1. Peter H. Schultz and Donald E. Gault, "Seismic Effects from Major Basin Formations on the Moon and Mercury," The Moon 12, 159-177, 1975.

2. Peter H. Schultz and Donald E. Gault, "Seismically induced modification of lunar surface features," Proc. Lunar Sci. Conf. 6th, 1975.

The Moon **12** (1975) 159–177.

SEISMIC EFFECTS FROM MAJOR BASIN FORMATIONS ON THE MOON AND MERCURY

PETER H. SCHULTZ and DONALD E. GAULT
Space Science Division, NASA Ames Research Center, Moffett Field, Calif., U.S.A.

(Received 8 October, 1974)

Abstract. Grooved and hilly terrains occur at the antipode of major basins on the Moon (Imbrium, Orientale) and Mercury (Caloris). Such terrains may represent extensive landslides and surface disruption produced by impact-generated *P*-waves and antipodal convergence of surface waves. Order-of-magnitude calculations for an Imbrium-size impact (10^{34} erg) on the Moon indicate *P*-wave-induced surface displacements of 10 m at the basin antipode that would arrive prior to secondary ejecta. Comparable surface waves would arrive subsequent to secondary ejecta impacts beyond 10^3 km and would increase in magnitude as they converge at the antipode. Other seismically induced surface features include: subdued, furrowed crater walls produced by landslides and concomitant secondary impacts; emplacement and leveling of light plains units owing to seismically induced 'fluidization' of slide material; knobby, pitted terrain around old basins from enhancement of seismic waves in ancient ejecta blankets; and perhaps the production and enhancement of deep-seated fractures that led to the concentration of farside lunar maria in the Apollo-Ingenii region.

NASA—118(III)

Proc. Lunar Sci. Conf. 6th (1975) p. 000-000
Printed in the United States of America

Seismically induced modification of lunar surface features

PETER H. SCHULTZ

University of Santa Clara, Santa Clara, California 95053

DONALD E. GAULT

NASA Ames Research Center, Moffett Field, California 94035

Abstract—The formation of large impact craters and basins produced not only large volumes of ejecta but also catastrophic seismic waves. Theoretical models, extrapolation of terrestrial explosion data, and extrapolation of lunar impact data suggest surface displacements of 1–10 m at four crater radii from a Copernicus-size impact (4×10^{26} ergs). Independent estimates of impact-generated stresses indicate that regions within 4 crater radii of an impact will receive shock waves with pressures exceeding 1 kbar. Greater areas also may receive shock effects as elastic waves following deep ray paths transform into shock waves near the surface. Additional seismic energy will be generated by impacts from secondary ejecta. The resulting large and long-lasting surface movement may contribute to the subdued appearance of the continuous ejecta blanket and secondary craters around large impact craters and to the degradation of small craters outside these zones.